Earthq Sci (2013) 26(5):293–299
DOI 10.1007/s11589-013-0028-x

Processes of the displacement field change of the 2009 April 6 M_W6.3 L'Aquila earthquake using persistent scatterer and small baseline methods

Sanming Luo · Liming Fu · Shuang Zhu · Qinglong He · Wenni Wan · Bo Yang

Received: 14 January 2013 / Accepted: 17 October 2013 / Published online: 16 November 2013

Abstract Using a time series method that combines both the persistent scatterer and small baseline approaches, we analyzed 9 scenes Envisat ASAR data over the L'Aquila earthquake, and obtained a Shocke's displacement field and its evolution processes. The results show that: (1) Envisat ASAR clearly detected the whole processes of displacement field of the L'Aquila earthquake, and distinct variations at different stages of the displacement field. (2) Preseismic creep displacement → displacement mutation when faulting → constantly slowed down after the earthquake. (3) The area of the strongest deformation and ground rupture was a low-lying oval depression region to the southeast. Surface faulting within a zone of about 22 km × 14 km, with an orientation of 135°, occurred along the NW-striking and SW-dipping Paganica-S. Demetrio normal fault. (4) In analyzing an area of about 54 km × 59 km, bounded by north–south axis to the epicenter, the displacement field has significant characteristics of a watershed: westward of the epicenter shows uplift with maximum of 130 mm in line-of-sight (LOS), and east of the epicenter was a region with 220 mm of maximum subsidence in the LOS, concentrating on the rupture zone, the majority of which formed in the course of faulting and subsequence.

Keywords PS method · SB method · Incorporating processing · Time series · L'Aquila earthquake · Displacement field

S. Luo (✉) · L. Fu · S. Zhu · Q. He · W. Wan · B. Yang
First Crust Monitoring and Application Center, China Earthquake Administration, Tianjin 300180, China
e-mail: luosanming@yahoo.com

1 Introduction

An M_W6.3 earthquake occurred on 6 April 2009 close to the city of L'Aquila in the central Apennines at a depth of about 9 km. The main shock was followed by thousands of aftershocks, of which two large events were M_W5.6 and 5.4 on April 7 and 9, respectively. It caused heavy damage in the town of L'Aquila with inhabitants of 73,000 and in many neighboring villages, and resulted over 300 fatalities and thousands of injures and tens of thousands homeless.

After the earthquake, researchers studied and interpreted this event using various methods and data sources from different fields, and a lot of results have been documented. Atzori et al. defined the geometric and kinematic characteristics of the fault activated during the earthquake by finite fault inversion of DInSAR co-seismic displacement interferograms, integrated with 30 GPS site displacements. The results showed that the best-fit solution for the main shock was addressed by a normal fault ~16 km long and ~12 km wide, with a small right-lateral component, dipping 47°SW with a maximum slip of ~90 cm (Atzori et al. 2009). Four days before the main quake, Anzidei et al. increased the existing permanent GPS network with five GPS stations bordering the L'Aquila basin. The maximum horizontal and vertical coseismic ground displacements surveyed at these stations were ~10.39 and ~−15.64 cm, respectively. With a nonlinear inversion of the geodetic data, the source geometry was best fitted as a 13 km × 15.7 km rectangular fault, SW-dipping at 55° ± 1.8° (Anzidei et al. 2009). Optimal source parameters of the earthquake from InSAR observations showed that this quake is associated with a buried SW-dipping normal fault with the epicenter at (13.4506°E, 42.3580°N), a strike of 141.3°, a dip of 50°, and the maximum slip of 1.2 m at the depth of 6.1 km (Feng et al. 2010). Walters

et al. (2009) used InSAR and body-wave seismology to determine independent source parameters for the event and confirmed that the quake ruptured a SW-dipping normal fault with ~0.6–0.8 m slip, and the L'Aquila earthquake occurred in an area with a marked seismic deficit relative to geodetically determined strain accumulation. Di Luccio et al. (2009) relocated the October 2008–6 April 2009 foreshocks and about 2,000 aftershocks occurred between 6 and 30 April 2009 by applying a double-difference technique. Using high-resolution foreshocks and aftershocks location, the geometry of fault segments was presented (Chiaraluce et al. 2011). L'Aquila earthquake ruptured an approximately 18-km-long SW-dipping normal fault. The aftershock area extended for a length of more than 35 km. Surface faulting occurred along the SW-dipping Paganica fault with a continuous extent of ~2.5 km (EMERGEO Working Group 2010).

However, an earthquake case, from its seismogenic to the rupture and the effect after the quake, is a very complex geophysics process. For a long time, seismologists have been doing a lot of works to explore the physical and tectonic mechanism of this process. In this paper, a new algorithm, StaMPS (Stanford Method for Persistent Scatterer) introduced by Hooper et al. (2007), that combines both PS and SB approaches to maximize the spatial sampling of useable signals was used. StaMPS has the advantage of spatial correlation between pixels in order to identify the most probable PS pixels and improve the spatial sampling. This is important not only because the resolution of any deformation signal is increased, but also because it allows for more reliable estimation of integer phase-cycle ambiguities present in the phase-unwrapping data. As a test case, the algorithm was applied to the L'Aquila earthquake that occurred on 6 April 2009 in Italy.

2 Methods

PS pixels are identified from interferograms optimized for PS analysis, and the identification methods for SDFP is that it operates on single-look images to identify single-look SDFP pixels directly (Hooper et al. 2007; Hooper 2008). In order to derive the deformation field, integer phase-cycle ambiguities, measured modulo 2π radians, must be estimated. A well-known process is phase unwrapping (Chen 2001; Hooper and Zebker 2007). The issue of phase unwrapping is inherently non-unique, but increasing the spatial sampling reduces the chances of spatial-aliasing and thereby increasing the chances of success. The selected PS and SDFP pixels are, therefore, combined before this step to maximize the reliability of the unwrapped phase. In order to achieve this, the equivalent SB interferogram phase, $\psi^{\mathrm{SB}}_{x,i}$, for PS pixels by recombination of single-master interferogram phase, was calculated:

$$\psi^{\mathrm{SB}}_{x,i} = W\left\{\psi^{\mathrm{SM}}_{x,s} - \psi^{\mathrm{SM}}_{x,m}\right\}, \quad (1)$$

where $\psi^{\mathrm{SM}}_{x,s}$ is the single-master phase for the small baseline slave, $\psi^{\mathrm{SM}}_{x,m}$ is the single-master phase for the small baseline master, and $W\{\cdot\}$ is the wrapping operator.

In order to combine the datasets the equivalent SB interferogram, the phase is calculated for the PS pixels by recombination of single-master interferogram phase. The equivalent SB phase is different to that extracted from the small baseline interferograms directly, because spectral filtering has not been applied. This is usually lower than the value calculated from the single-master interferogram phase, where the master contribution to the decorrelation term is present in every interferogram and does not, therefore, contribute to the variation. The SB interferogram phase from both PS and SDFP pixels is then combined. When a pixel occurs in both datasets, a weighted mean value for the phase is calculated by summing the complex signal from both datasets, with the amplitude of each fixed to an estimate of the signal-to-noise ratio (Just and Bamler 1994) for the pixel in that dataset.

The phase of the combined dataset is corrected using the estimate of spatially uncorrelated look angle error calculated in the selection steps. The method is then applied to unwrap the resulting phase of each combined SB interferogram. Phase unwrapping of SB interferograms, which cover short time intervals, as opposed to single-master interferograms has the added advantage of reducing spatial-aliasing in the case of high deformation rates.

The unwrapped phase of the SB interferograms must be inverted to derive a time series of phase changes for each pixel. Berardino et al. performed the inversion using singular value decomposition, imposing an extra minimum-norm constraint (Chen 2001). As there are no isolated clusters of interferograms in this analysis, this extra constraint is not required and the unwrapped phase was

Table 1 Ascending orbit data processed with PS for the L'Aquila earthquake (Track: 401)

No.	Orbit	Date	Sensor	$B_\perp$ (m)	f_{DC} (Hz)	Days	Remark
1	34523	2008-10-06	Envisat	0	−560.63	0	Master
2	35204	2008-11-10	Envisat	467	−551.44	35	Slave
3	36026	2009-01-19	Envisat	437	−555.95	105	Slave
4	36527	2009-02-23	Envisat	−3	−550.54	140	Slave
5	37028	2009-03-30	Envisat	581	−553.11	175	Slave
6	37529	2009-05-04	Envisat	−145	−557.86	210	Slave
7	38030	2009-06-08	Envisat	−144	−564.12	245	Slave
8	38531	2009-07-13	Envisat	400	−549.31	280	Slave
9	39533	2009-09-21	Envisat	626	−548.84	350	Slave

inverted in a least-squares fashion, similar to Schmidt and Bürgmann (Hooper and Zebker 2007). The model phase retrieved is then the phase of each pixel relative to an arbitrary reference pixel and master image. To check that the phase for all SB interferograms contributing to each final single-master interferogram is consistent, the residual phase between the SB interferograms and the phase predicted by the model single-master interferograms was calculated. Residuals of up to 2π are expected for individual pixels, due to local phase-unwrapping errors, but any spatially correlated residuals imply systematic phase-unwrapping errors. If this is the case, problem interferograms can be identified and their phase unwrapped more carefully, or they can be dropped from the inversion if the redundancy of the SB interferograms allows.

Table 2 Ascending orbit data processed with SB for the L'Aquila earthquake (Track: 401)

No.	Master	Slave	Sensor	$B_\perp$ (m)	f_{DC} (Hz)	Days
1	2008-10-06	2008-11-10	Envisat	467	−560.63	35
2	2008-10-06	2009-01-19	Envisat	436	−555.95	105
3	2008-10-06	2009-02-23	Envisat	−3	−550.54	140
4	2008-10-06	2009-05-04	Envisat	−144	−557.86	210
5	2008-10-06	2009-06-08	Envisat	−143	−564.12	245
6	2008-10-06	2009-07-13	Envisat	399	−549.31	280
7	2008-11-10	2009-01-19	Envisat	−31	−555.95	70
8	2008-11-10	2009-02-23	Envisat	−470	−550.54	105
9	2008-11-10	2009-03-30	Envisat	122	−553.11	140
10	2008-11-10	2009-07-13	Envisat	−68	−549.31	245
11	2008-11-10	2009-09-21	Envisat	164	−548.84	315
12	2009-01-19	2009-02-23	Envisat	−439	−550.54	35
13	2009-01-19	2009-03-30	Envisat	153	−553.11	70
14	2009-01-19	2009-07-13	Envisat	−37	−549.31	175
15	2009-01-19	2009-09-21	Envisat	195	−548.84	245
16	2009-02-23	2009-05-04	Envisat	−141	−557.86	70
17	2009-02-23	2009-06-08	Envisat	−140	−564.12	105
18	2009-02-23	2009-07-13	Envisat	402	−549.31	140
19	2009-03-30	2009-07-13	Envisat	−190	−549.31	105
20	2009-03-30	2009-09-21	Envisat	42	−548.84	175
21	2009-05-04	2009-06-08	Envisat	1	−564.12	35
22	2009-07-13	2009-09-21	Envisat	232	−548.84	70

3 Data processing for L'Aquila Earthquake

The combined MT-InSAR method described in this paper was applied to 9 scenes of ascending data acquired by Envisat ASAR satellites over the L'Aquila earthquake from October 2008 to September 2009. The details about images with two methods are shown in Tables 1 and 2, respectively.

The same certainty threshold of 99 % for pixel selection was used for both methods. Within an area of 54 km × 59 km, using the PS method, 88,245 PS pixels were identified as opposed to 17,916 pixels with the SB method. Of the selected pixels, 62,460 were selected by both methods. The pixels combined by both methods were called SB for convenience of description in this paper.

Results from SB are shown in the following figures. Figures 1 and 2 are timing interferograms from wrapping data and unwrapping data, respectively. Figure 3 is the radar line-of-sight (LOS) displacement field, derived by SB targets. The fit faults in the figure are cited from the literature (Atzori et al. 2009), and the focal mechanism solutions of main event and foreshocks and aftershocks are followed Pondrelli et al. (2009). Three small rectangular frames A, B, and C in Fig. 3 were three reference SB targets located in the rupture zone. UU and VV are profiles of the displacement field in Fig. 3. Figure 4 is time

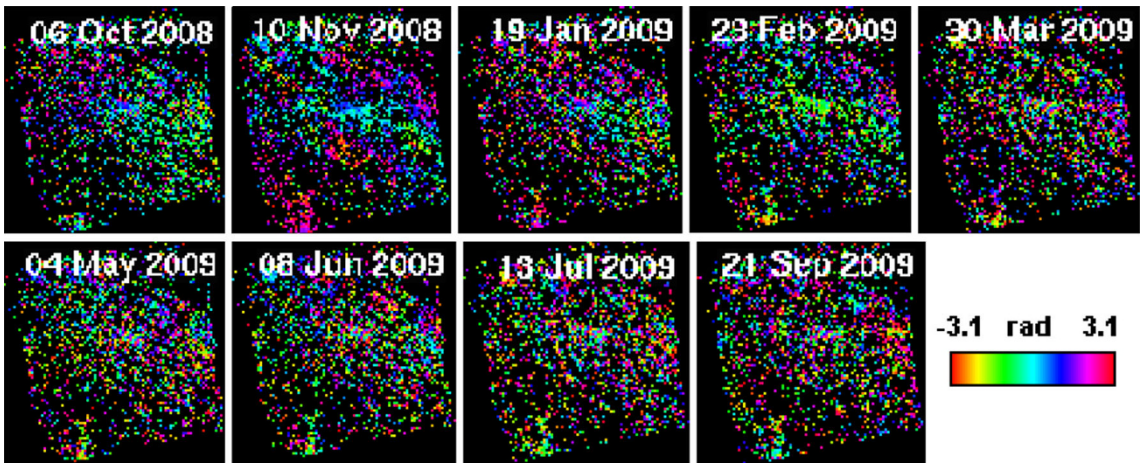

Fig. 1 SB time sequence interferograms wrapped phase in radar coordinates formed from ascending orbit data over L'Aquila

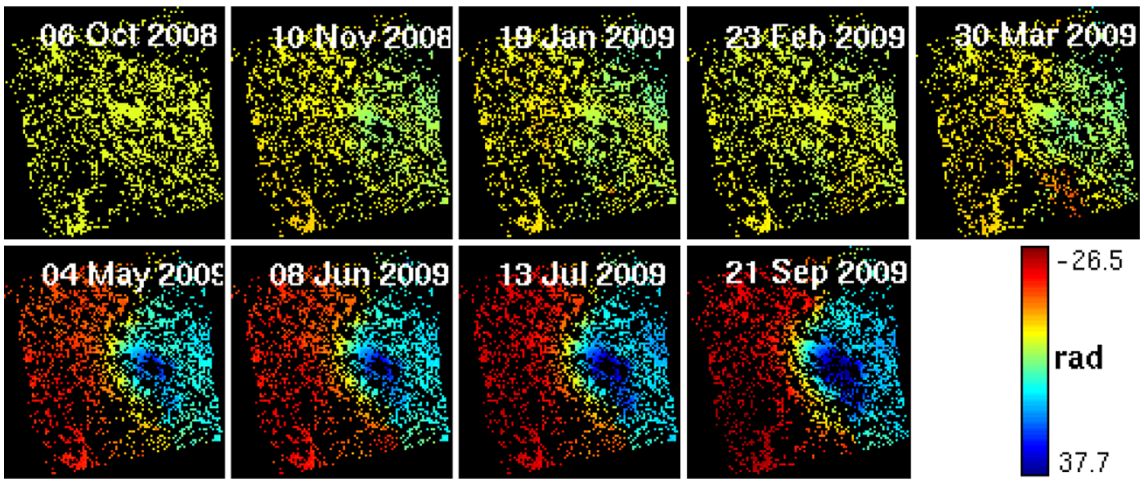

Fig. 2 SB time sequence displacement field unwrapped phase formed from ascending orbit data over L'Aquila, *dark blue section* represents rupture area

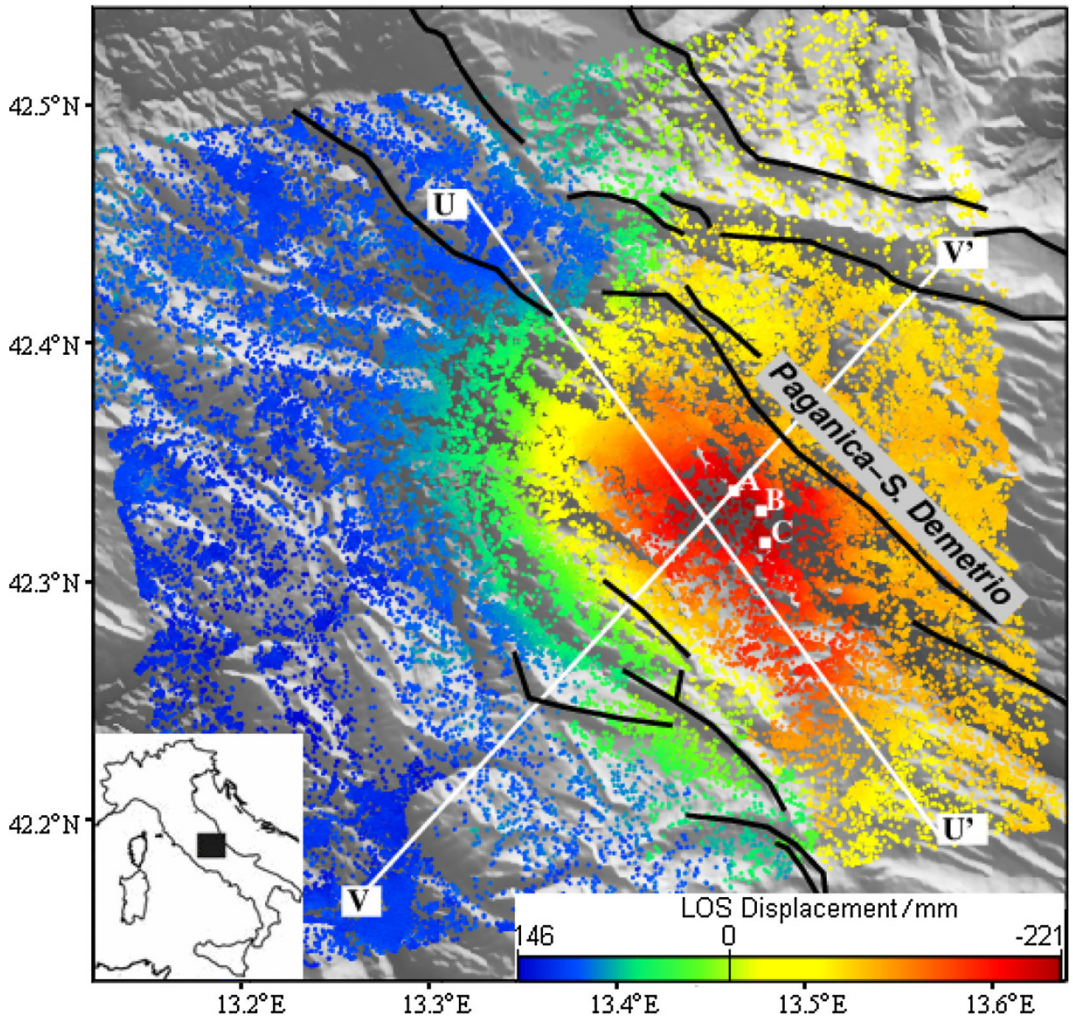

Fig. 3 LOS displacement field over L'Aquila zone from Oct 2008 to Sep 2009

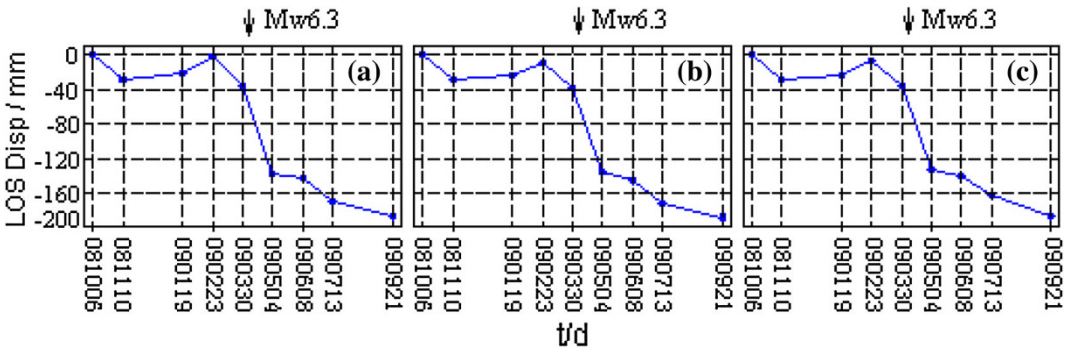

Fig. 4 Reference SB targets time sequence LOS displacement

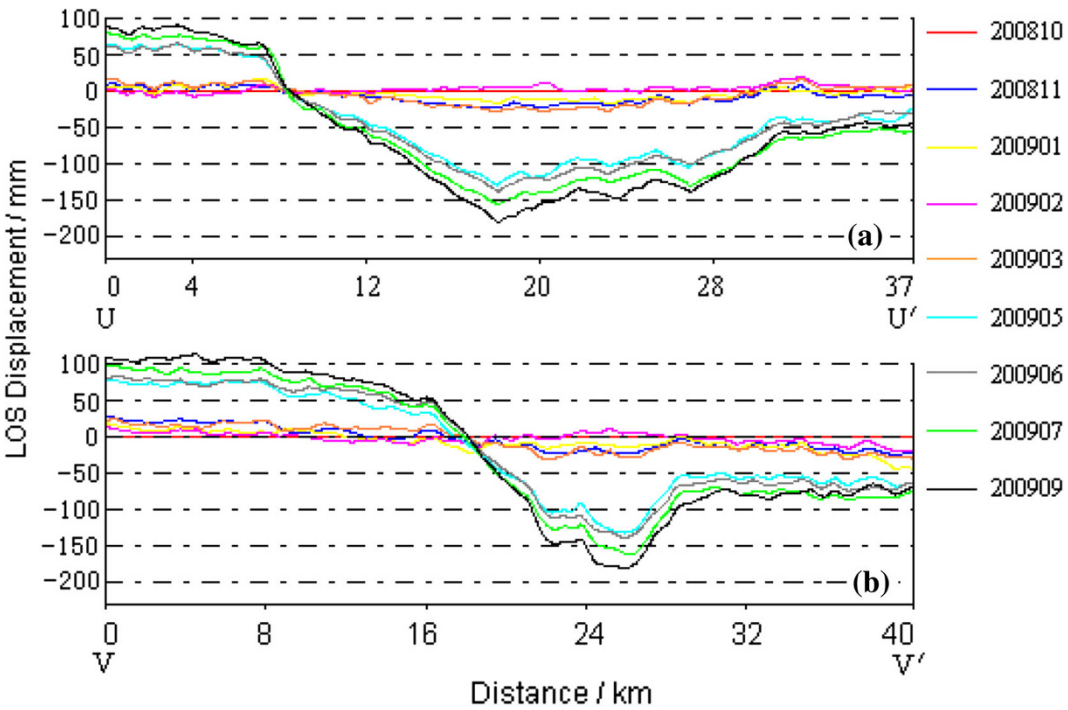

Fig. 5 Displacement field profiles of the L'Aquila earthquake. **a** Shows the profile along the *UU′* and **b** along the *VV′*

sequence chart of three reference SB targets A, B, and C. Figure 5 is a profile chart of UU′ and VV′, shown in Fig. 3. Figure 6 is a reconstruction of the propagating direction and the deformation processes of the rupture zone based on Delaunay triangulation algorithm for SB targets.

4 Discussion and conclusions

After the earthquake, researchers studied and interpreted this event using various methods and data sources from different fields. In this paper, based on previous work and by applying time sequence method to 9 repeat-pass ASAR images, we represented the whole evolution processes of the displacement field of the L'Aquila earthquake. The results of this paper demonstrated the different deformation characteristics of the displacement field in the different phases caused by the earthquake during the imaging period. The deformation caused by different shocks (i.e., the main shock and significant aftershocks), and the deformation characteristics in preseismic, coseismic, and postseismic of main shock also were represented. All of these results are consistent with the results derived by descending data (Luo et al. 2012), PS method (Luo et al. 2012) and SB method (Luo et al. 2011), respectively. The initial thought from the paper is as follows.

(i) In the half year before the earthquake, the surface of the epicenter has already begun to change slowly, after the earthquake, subsidence in the rupture zone increased with the large magnitude. The ground

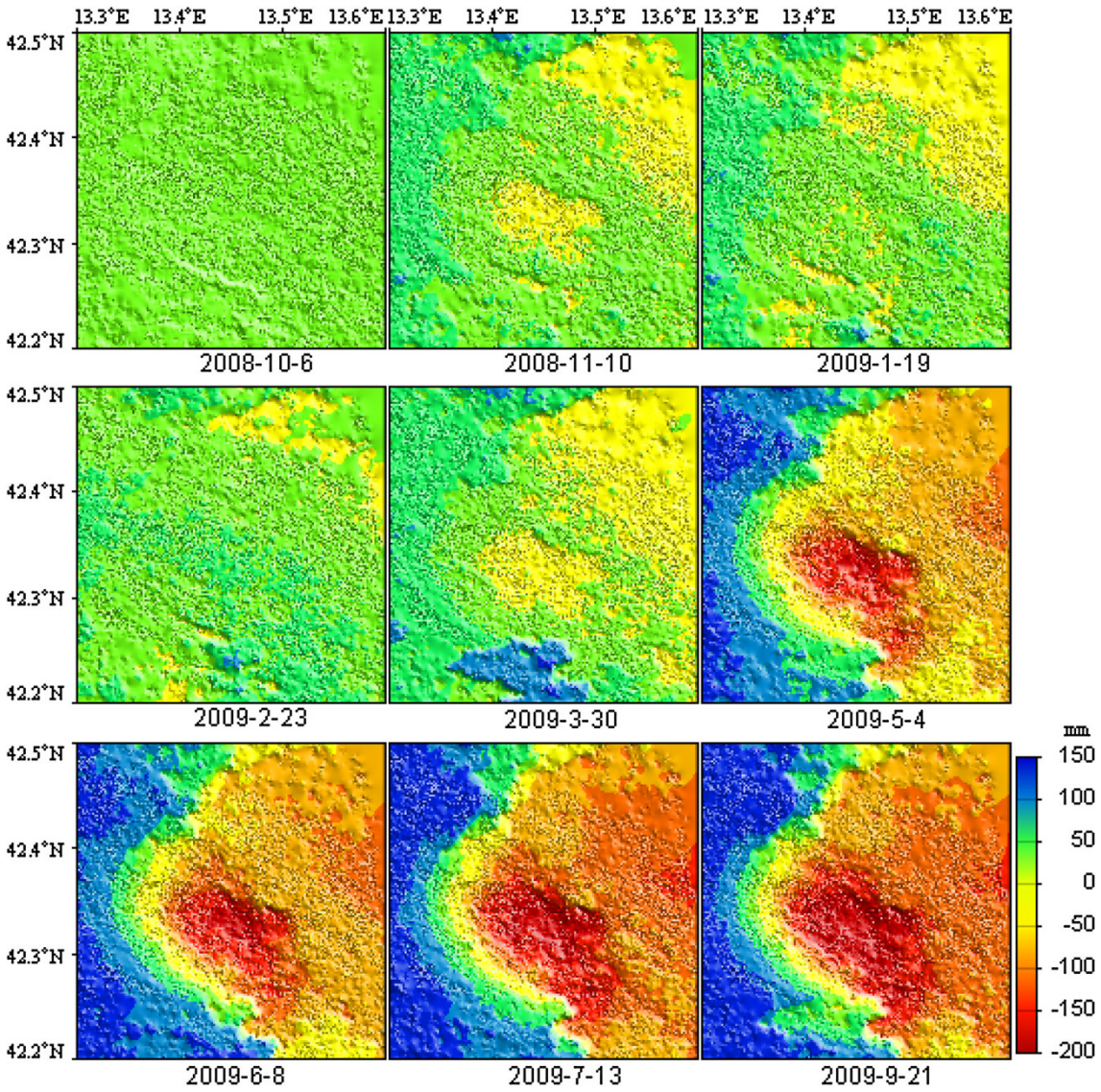

Fig. 6 Reconstruction of the propagating direction and the deformation processes of rupture zone based on the Delaunay triangulation algorithm for SB targets

cracking is asymmetrical since the deformed area is significantly expanded to the southeast. The deformed area is about 310 km^2 with a maximum length of 22 km, trending NW–SE along the direction of the rupture plane, and a maximum width of 14 km, trending NE–SW. A large subsidence bowl was formed in the epicenter.

(ii) In 2003, Hunstad et al. (2003) processed the GPS data and triangulation network observation data since 1860, and their results show that the significant strain accumulated over the past 130 years may not have been released in the past by earthquakes in the Apennines. Although the L'Aquila earthquake that occurred on 6 April 2009 is the strongest event since the M7.0 Fucino earthquake in the central of Italy in 1915 (Falcucci et al. 2009), the results in this paper suggest that this area might be susceptible to a stronger earthquake in the future since the L'Aquila shock was not strong enough to release the long-term strain accumulated in the area.

(iii) According to the reference PS sequence in Fig. 4, we can conclude that if regardless of the creep variables of the displacement field before earthquakes, the displacement of the fracture location from March to September in 2009 is about 165 mm, considering the radar LOS is 23°, vertical displacement value of the displacement field is consistent with GPS results (Anzidei et al. 2009).

(iv) Synthetic aperture radar interferometry can obtain the change information and evolution processes of

surface "field" without any artificial targets. This promises the continuity of the data chain, and the continuous information can be obtained even in the rupture zone. This is impossible using conventional geodetical methods. Thus, the work in this paper has provided a comprehensive case for understanding new methods for earthquake forecasting with time sequence DInSAR.

Acknowledgments The authors would like to thank the European Space Agency for providing data, and also the precision orbit data provided by the Netherlands Delft University of Technology. This work was supported by Director Foundation of the Institute of Seismology, China Earthquake Administration(IS201266111), the Seism Science & Technology Spark Program of China Earthquake Administration(XH13036) and Earthquake Industry Research Special Project (201308009).

References

Anzidei M, Cannelli V, Devoti R et al (2009a) Coseismic deformation of the destructive April 6, 2009 L'Aquila earthquake (Central Italy) from GPS data. Geophys Res Lett 36:L17307. doi:10.1029/2009GL039145

Anzidei M, Cannelli V, Devoti R et al (2009b) Coseismic deformation of the destructive April 6 2009 L'Aquila earthquake (Central Italy) from GPS data. Geophys Res Lett 36:L17307. doi:10.1029/2009GL039145

Atzori S, Hunstad I, Chini M et al (2009a) Finite fault inversion of DInSAR coseismic displacement of the 2009 L'Aquila earthquake (Central Italy). Geophys Res Lett 36:L15305. doi:10.1029/2009GL039293

Atzori S, Hunstad I, Chini M, Salvi S et al (2009b) Finite fault inversion of DInSAR coseismic displacement of the 2009 L'Aquila earthquake (Central Italy). Geophys Res Lett 36:L15305. doi:10.1029/2009GL039293

Chen CW (2001) Statistical-cost network-flow approaches to two-dimensional phase unwrapping for radar interferometry. PhD thesis, Stanford University

Chiaraluce L, Valoroso L, Piccinini D et al (2011) The anatomy of the 2009 L'Aquila normal fault system (Central Italy) imaged by high resolution foreshock and aftershock locations. J Geophys Res. doi:10.1029/2011JB008352

Di Luccio F, Ventura G, Di Giovambattista R et al (2009) Normal faults and thrusts reactivated by deep fluids: the 6 April 2009 Mw 6.3 L'Aquila earthquake, Central Italy. J Geophys Res 115(B6):B06315. doi:10.1029/2009JB007190

EMERGEO Working Group (2010) Evidence for surface rupture associated with the Mw 6.3 236 L'Aquila earthquake sequence of April 2009 (Central Italy). Terra Nova 22:43–51

Falcucci E, Gori S, Peronace E, Fubelli G et al (2009) The Paganica fault and surface coseismic ruptures caused by the 6 April 2009 earthquake (L'Aquila, Central Italy). Seismol Res Lett 80(6):940–950

Feng WP, Li ZH, Li CL (2010) Optimal source parameters of the 6 April 2009 Mw 6.3 L'Aquila, Italy earthquake from InSAR observations. Progr Geophys 25(5):1550–1559 (in Chinese with English abstract)

Hooper A (2008) A multi-temporal InSAR method incorporating both persistent scatterer and small baseline approaches. Geophys Res Lett 35:L16302. doi:10.1029/2008GL034654

Hooper A, Zebker H (2007) Phase unwrapping in three dimensions with application to InSAR time series. J Opt Soc Am A 24:2737–2747

Hooper A, Segall P, Zebker H (2007) Persistent scatterer interferometric synthetic aperture radar for crustal deformation analysis, with application to Volca'n Alcedo, Gala'pagos. J Geophys Res 112:B07407. doi:10.1029/2006JB004763

Hunstad I, Selvaggi G, D'Agostino N, England P, Clarke P, Pierozzi M (2003) Geodetic strain in peninsular Italy between 1875 and 2001. Geophys Res Lett 30:1181. doi:10.1029/2002GL016447

Just D, Bamler R (1994) Phase statistics of interferograms with applications to synthetic-aperture radar. Appl Opt 33(20):4361–4368

Luo S, Yang G et al (2011) Detection based on SB-dinsar time series of earthquake deformation process. J Geod Geodyn 31(6):15–19 (in Chinese with English abstract)

Luo S, Yang G et al (2012) Analysis of deformation process of L'Aquila earthquake detected by PSInSAR. Geomat Inf Sci Wuhan Univ 37(5):602–605, 609 (in Chinese with English abstract)

Luo S, Dong Y et al (2012) Displacement field characteristics on L'Aquila earthquake from PSInSAR time series. Prog Geophys 27(4):1307–1315 (in Chinese with English abstract)

Pondrelli S, Salimbeni S, Morelli A, Ekstrom G, Olivieri M, Boschi E (2009) Seismic moment tensors of the, L'Aquila (Central Italy), earthquake sequence. Geophys J Int. doi:10.1111/j.1365-246X.2009.04418.x

Walters RJ, Elliott JR, D'Agostino N et al (2009) The 2009 L'Aquila earthquake (Central Italy): a source mechanism and implications for seismic hazard. Geophys Res Lett 36(17):L17312. doi:10.1029/2009GL039337